Geophysical Research Letters

Supporting Information for

Cave dripwaters capture the 2015 – 2016 El Niño event in N. Borneo

Shelby A. Ellis*[1], Kim M. Cobb[1], Jessica W. Moerman[2], Judson W. Partin[3], A. Landry Bennett[1], Jenny Malang[4], Hein Gerstner[4], Andrew A. Tuen[5]

[1]School of Earth and Atmospheric Sciences, Georgia Institute of Technology, Atlanta, Georgia USA, [2]Human Origins Program, National Museum of Natural History, Smithsonian Institution, Washington, DC USA, [3]Institute for Geophysics, Jackson School of Geosciences, University of Texas at Austin, Austin, Texas USA, [4]Gunung Mulu National Park, Sarawak, Malaysia, [5]Institute of Biodiversity and Environmental Conservation, Universiti Malaysia Sarawak, Sarawak, Malaysia

Contents of this file

Introduction

This supporting information encompasses figures and tables illustrating a research site map, rainfall and cave dripwater observations specific to individual El Niño Southern Oscillation events and seven cave dripwater spatial surveys, further model results from the main text, as well as comparisons between the first six years of published cave dripwater data (Moerman et al., 2014) versus the extended data set presented here. The supplemental figures and tables were created using MATLAB and Microsoft Office Powerpoint. The rainfall and cave dripwater timeseries including the spatial survey data were collected at Gunung Mulu National Park in Sarawak, Malaysia, Borneo between July 2006 and April 2018. The authors wish to express no conflicts of interests.

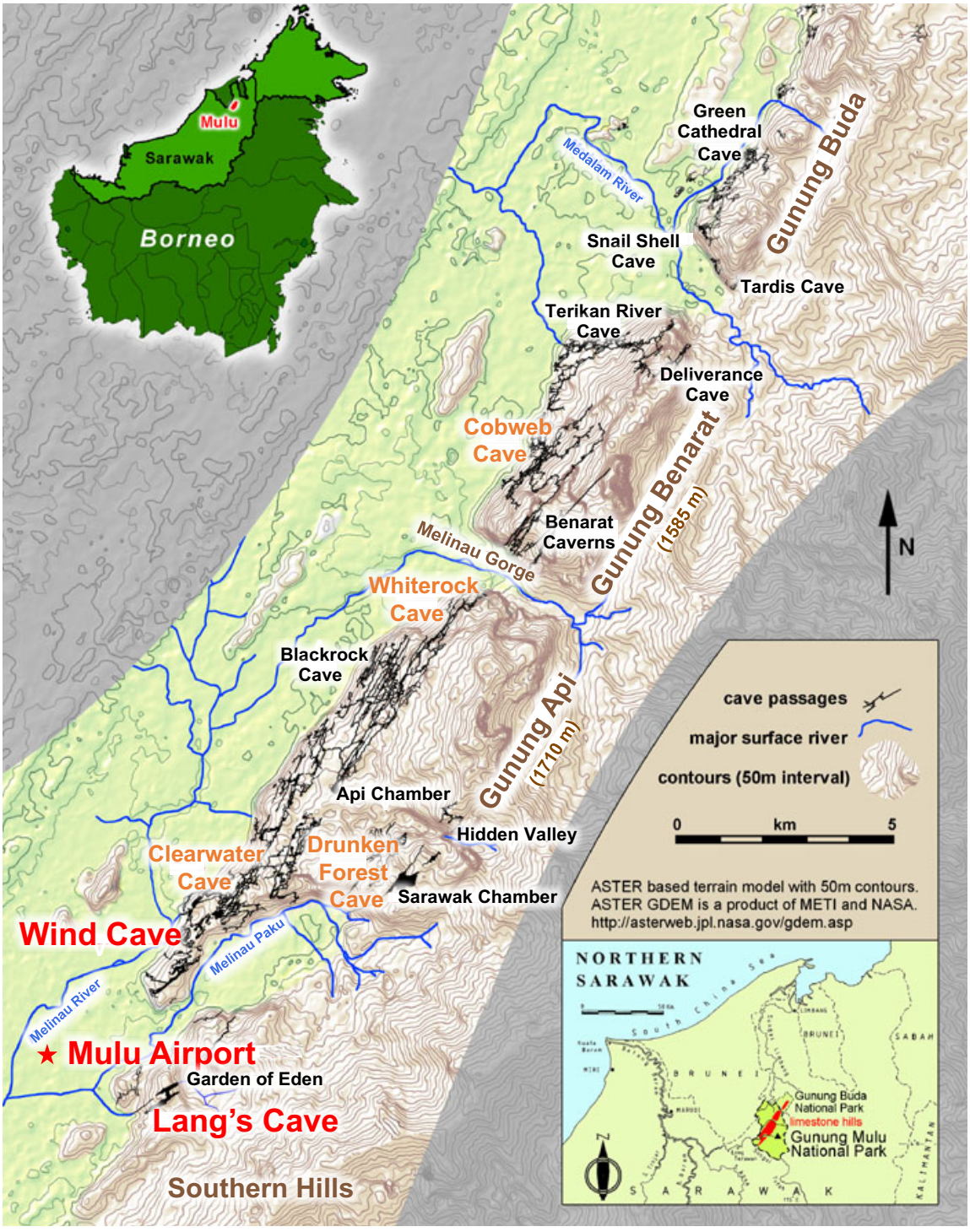

Figure S1 | Detailed map of Gunung Mulu National Park. Map on left adapted from Mulu Caves Project, with permission from Jerry Wooldridge that outlines Gunung Mulu National Park in Northern Sarawak, Borneo. The three cave dripwater and rainfall timeseries locations are in red, caves from seven spatial surveys of stalagmite and non-stalagmite forming drips written in orange, non-surveyed caves in black, mountains and gorges in brown, and rivers in blue.

Figure S2 | Photos of cave dripwater time series sites. (a) Lang's Cave (L2), (b) Wind Fast (WF), (c) Wind Slow (WS), and (d) WS. L2 drips onto ~2m tall stalagmite, WF drips onto edge of indented pool, and WS drips onto detrital bedrock. L2 is overlain by ~200m of limestone bedrock and WF and WS by ~100m of bedrock.

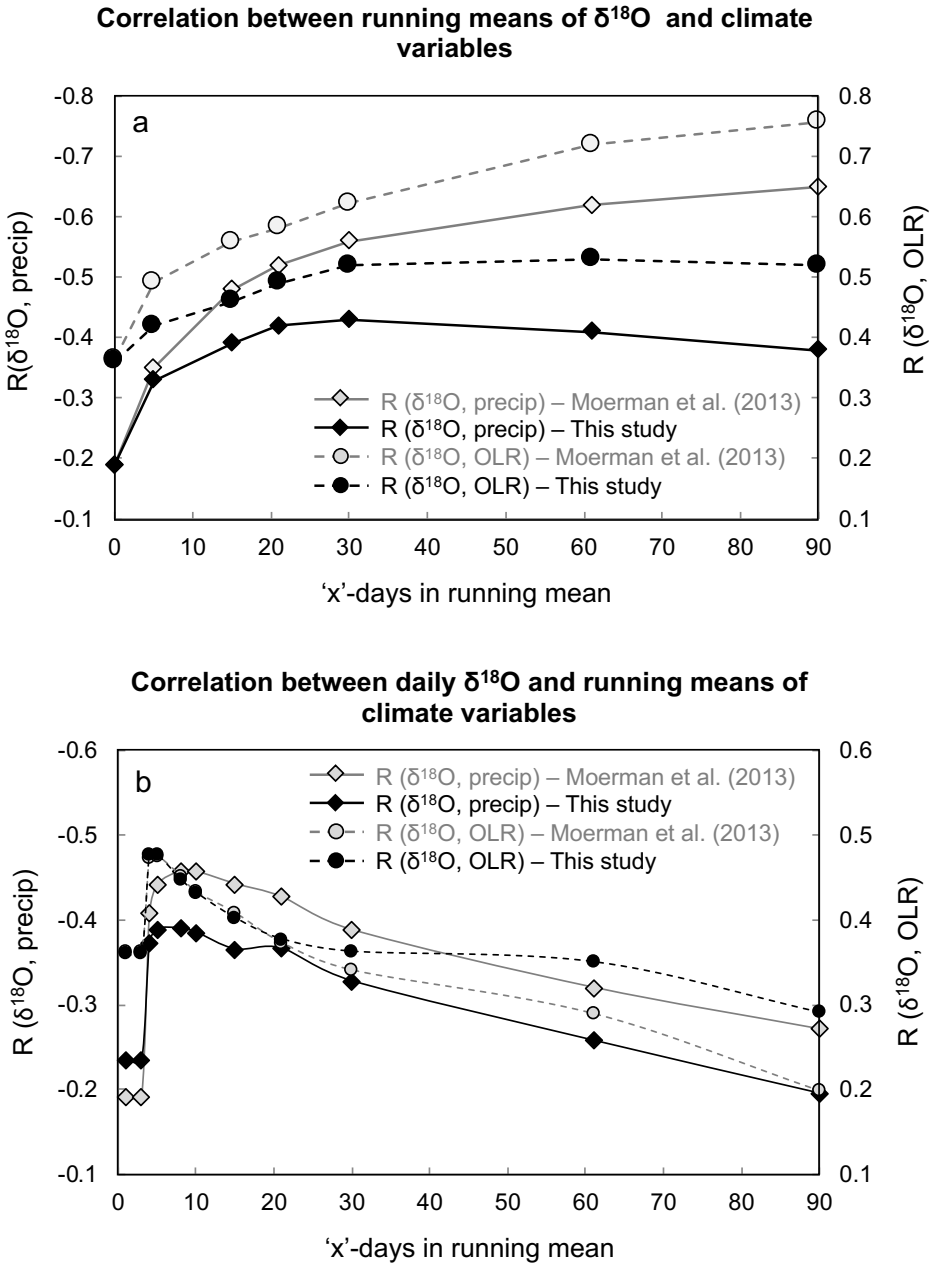

Figure S3 | Relationship between diurnal to monthly-scale variations in Mulu rainfall $\delta^{18}O$ versus local hydrological variables. (a) Correlation between 'x'-day running mean of Mulu rainfall $\delta^{18}O$ and 'x'-day running means of local Mulu precipitation amount (diamonds) and outgoing longwave radiation (OLR; circles), shown as the 2.5° x 2.5° grid box centered about 5°N, 115°E from https://www.esrl.noaa.gov/psd/data/gridded/data.interp_OLR.html. (b) Correlations between daily rainfall $\delta^{18}O$ values and 'x'-day running means of local Mulu precipitation amount (diamonds) and OLR (circles).

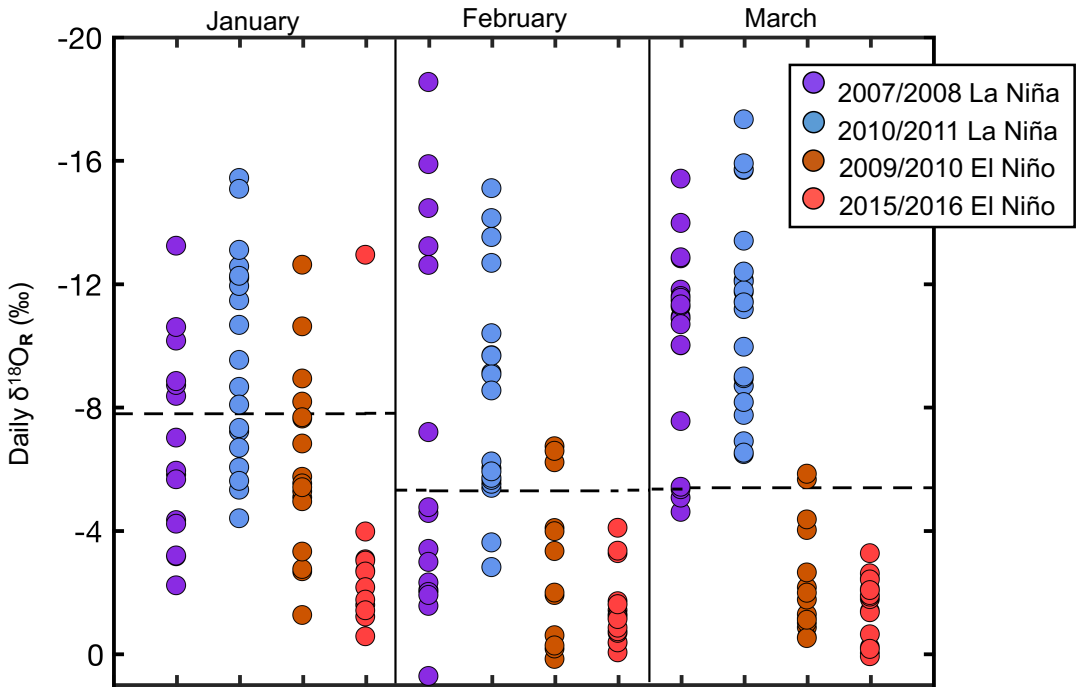

Figure S4 | Spread of local diurnal rainfall $\delta^{18}O$ in January, February and March (JFM) during four extreme ENSO events. Dashed lines indicate the respective monthly averages for the entire $\delta^{18}O$ data set (January = -7.8 ± 2.5‰; February = -5.3 ± 2.3‰; March = 5.4 ± 3.3‰). Note the JFM seasonal average for the entire rainfall time series is -6.1 ± 2.2‰. All values reported are 1σ. Y-axis is inverted.

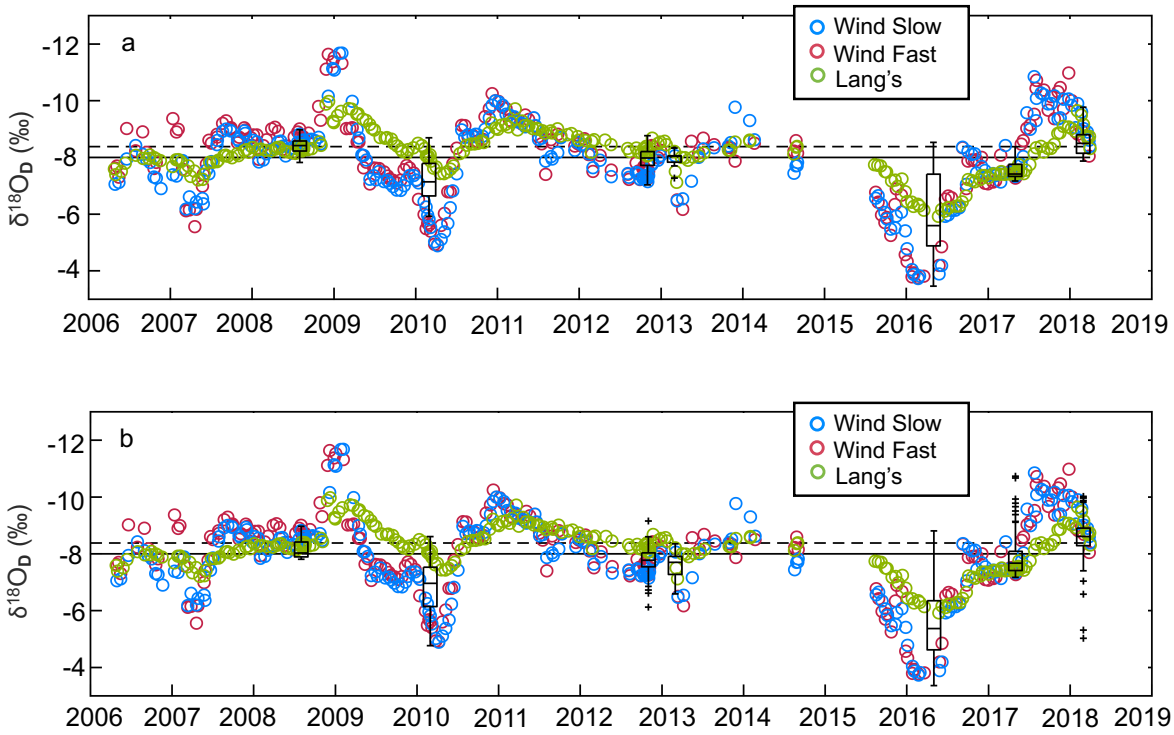

Figure S5 | Spatial cave dripwater $\delta^{18}O$ survey results against three Mulu cave dripwater $\delta^{18}O$ timeseries. Cave dripwater $\delta^{18}O$ observations denoted in colored circles from Wind Fast (WF, maroon), Wind Slow (WS, blue), and Lang's cave (L2, green). In both panels, boxes denote the 25 – 75% quartile range of surveyed cave dripwater $\delta^{18}O$ and whiskers as $\pm 2.7\sigma$ of distributed expedition data and outliers as any values outside of this standard deviation (black crosses). Mulu's amount-weighted rainfall $\delta^{18}O$ is denoted as a dashed line (-8.4 ± 2.4‰) and the combined mean from all three cave dripwater $\delta^{18}O$ time series as a solid line (-8.0 ± 1.2‰) in panels a and b. The standard deviation is reported as 1σ. (a) Stalagmite-forming and (b) non-stalagmite forming cave dripwater $\delta^{18}O$ during each survey as box and whisker plots. Y-axes are inverted in both panels.

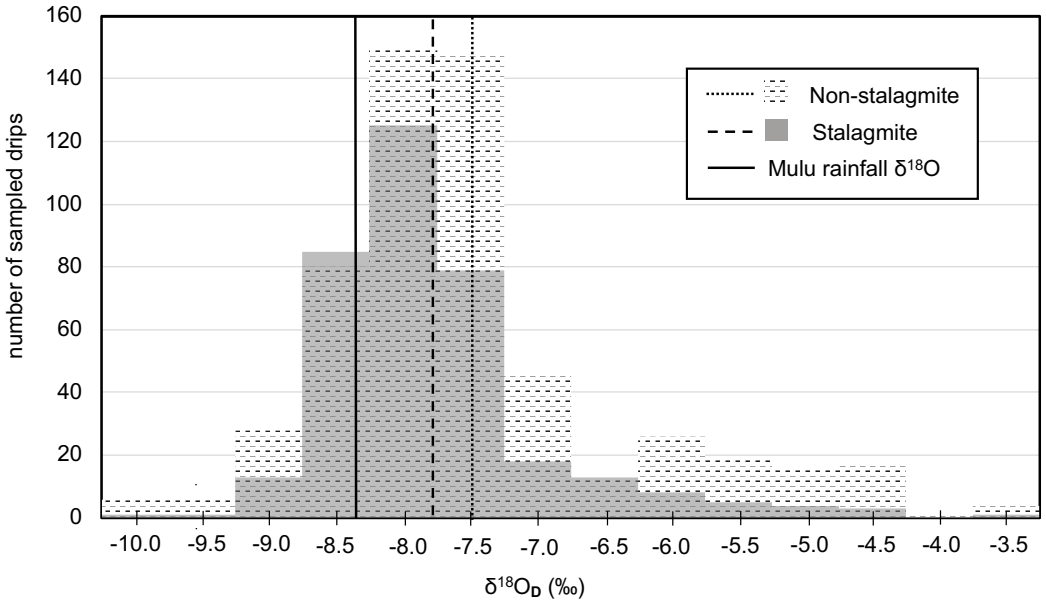

Figure S6 | Histogram of stalagmite vs. non stalagmite forming cave dripwater $\delta^{18}O$ values combined from seven spatial surveys. Non-stalagmite (stalagmite) forming drips are represented by dashed (grey) boxes. Non-stalagmite (N = 577) forming cave dripwater $\delta^{18}O$ mean is -7.5 ± 1.1‰ (dotted line) and the stalagmite (N = 356) forming cave dripwater $\delta^{18}O$ mean is -7.8 ± 0.8‰ (dashed line). Solid black line denotes the Mulu amount-weighted mean rainfall $\delta^{18}O$ (-8.4 ± 2.4‰). The standard deviations are reported as 1σ.

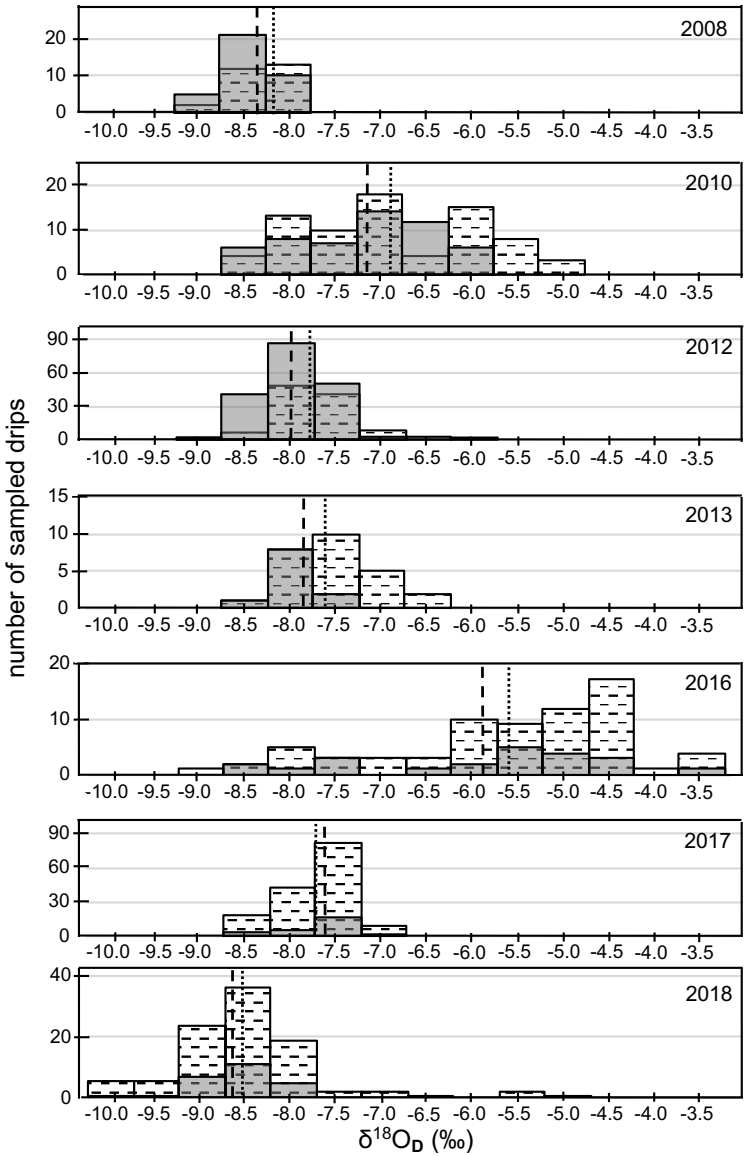

Figure S7 | Histograms from seven field spatial surveys over 2008 – 2018. Grey (dashed) boxes and dashed (dotted) lines indicate stalagmite (non-stalagmite) forming cave dripwater $\delta^{18}O$ and their corresponding mean value during each respective expedition. The y-axis displays number of sampled drips, and are different in scaling for each panel. All reported mean values are 1σ. Stalagmite forming drip means include August 2008 (-8.4 ± 1.4‰), February/March 2010 (-7.2 ± 0.7‰), October/November 2012 (-8.0 ± 0.3‰), March 2013 (-7.9 ± 0.3‰), May 2016 (-5.9 ± 1.4‰), May 2017 (-7.6 ± 0.3‰), and March/April 2018 (-8.6 ± 0.5‰). Non-stalagmite forming drip means include August 2008 (-8.2 ± 0.4‰), February/March 2010 (-6.9 ± 1.0‰), October/November 2012 (-7.8 ± 0.4‰), March 2013 (-7.6 ± 0.4‰), May 2016 (-5.6 ± 1.3‰), May 2017 (-7.7 ± 0.4‰), and March/April 2018 (-8.5 ± 0.8‰). All standard deviations are reported as 1σ.

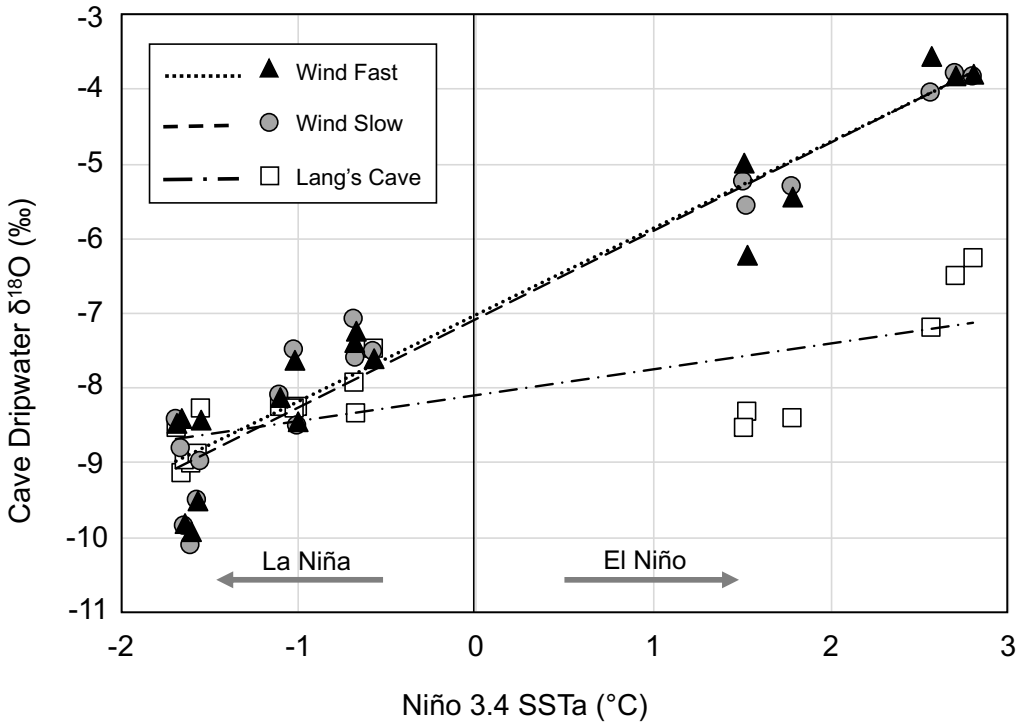

Figure S8 | Observed dripwater $\delta^{18}O$ excursions versus different ENSO events. Independent dripwater $\delta^{18}O$ observations from Wind Fast (WF, triangles), Wind Slow (WS, circles), and Lang's Cave (L2, squares) plotted against sea surface temperature anomalies (SSTa) in the Niño 3.4 region during specific time periods. Three observations were chosen at WF/WS(L2) approximately 3(10) months after the three most anomalous Niño 3.4 SSTa months, following the lag implied by the dripwater residence time calculations. Linear regressions plotted in black for WF (dotted; $R^2 = 0.94$), WS (dashed; $R^2 = 0.92$), and L2 (dash-dot; $R^2 = 0.54$).

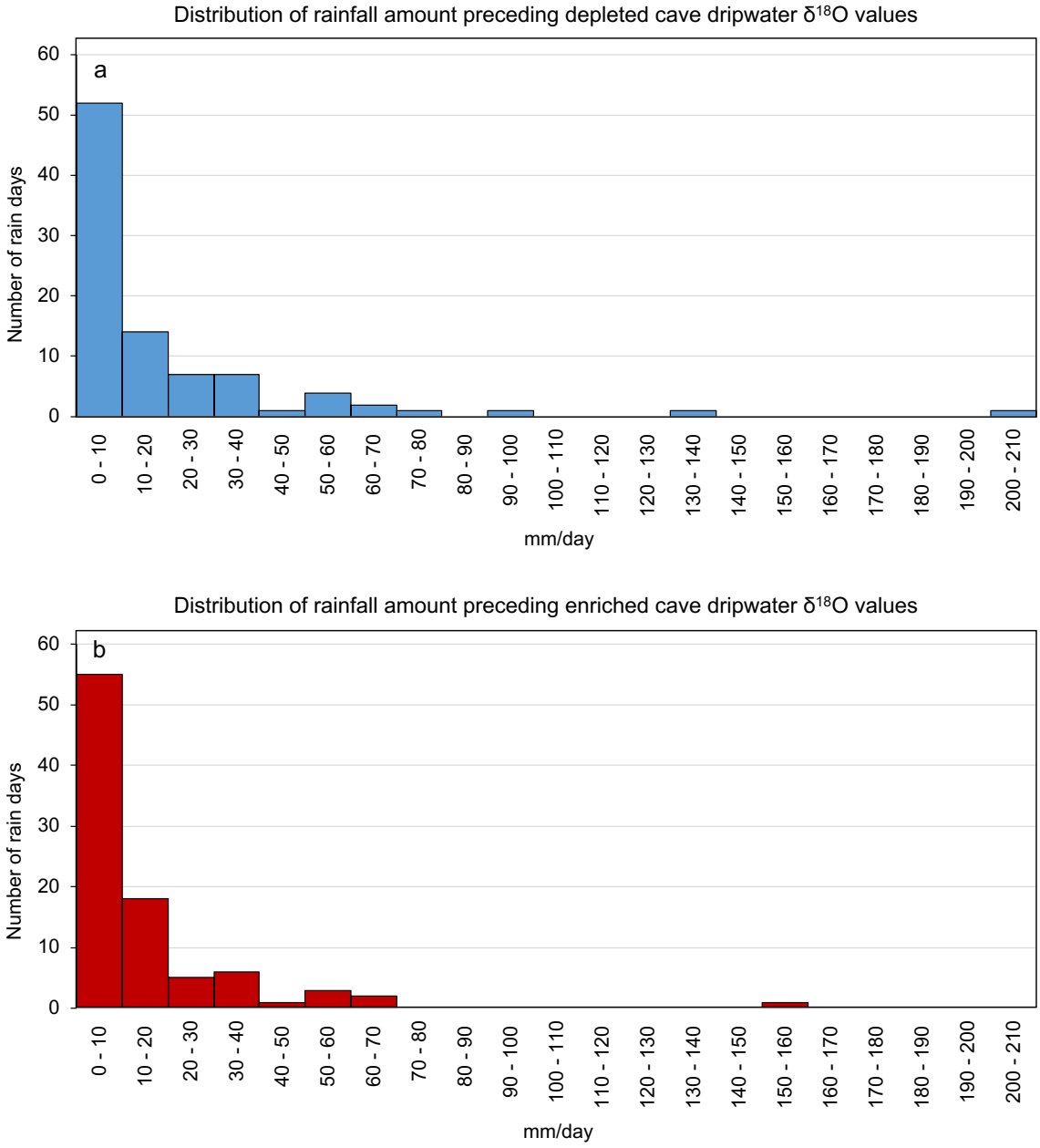

Figure S9 | Histogram comparison of potential hydraulic loading on anomalous cave dripwater $\delta^{18}O$ values. (a) Histogram of 90 days of Mulu rainfall amount (October, November, December) before anomalously depleted cave dripwater $\delta^{18}O$ observations (December 2008: Lang's Cave = -10.0‰, Wind Fast = -11.7‰, Wind Slow = -11.7‰). (b) Same as panel a, but 90 days of Mulu rainfall amount (March, April, May) before anomalously enriched Lang's Cave dripwater $\delta^{18}O$ observations in May 2016 (Lang's Cave, -5.9‰; enrichment for Wind Fast and Wind Slow occurred in February 2016 at -3.7‰ and -3.4‰, respectively).

Mulu rainfall $\delta^{18}O$ vs. Mulu rainfall amount		
'x'-days in running mean	**Moerman et al. 2013**	**This study**
0	-0.19	-0.21
15	-0.48	-0.39
21	-0.52	-0.42
30	-0.56	-0.43
61	-0.62	-0.41
90	-0.65	-0.38

Table S1 | Correlations of Mulu rainfall oxygen isotopes versus rainfall amount from this study and Moerman et al. (2013). The reported correlations are plotted in Figure S3 panel a.

ENSO Index	Pearson's correlation coefficient ($\delta^{18}O_R$)	Pearson's correlation coefficient (Rainfall Amount)
NIÑO1+2	0.46	-0.22
NIÑO3	0.58	-0.26
NIÑO3.4	0.62	-0.30
NIÑO4	0.64	-0.35
ONI	0.66	-0.28
SOI	-0.59	-0.33
El Niño Modoki Index	0.50	-0.34

Table S2 | Correlations with N. Borneo rainfall time series against various tropical Pacific climate indices. N. Borneo rainfall data is a 3 month centered average of each variable where $p<0.01$. All NIÑO data is from (*Huang et al.,* 2017) (ERSSTv5) found online at https://www.cpc.ncep.noaa.gov/data/indices/ersst5.nino.mth.81-10.ascii. ONI data was found online at https://www.esrl.noaa.gov/psd/data/correlation/oni.data, all SOI data found online at https://www.esrl.noaa.gov/psd/data/correlation/soi.data, and El Niño Modoki Index found online at http://www.jamstec.go.jp/frcgc/research/d1/iod/DATA/emi.monthly.txt.

BMM Reservoir A: Reservoir B (τ in weeks)	**Pearson's correlation coefficient**	**cumulative residual**
Best case (Figure 2B)	0.93	50.05
40:60 (41 weeks)	0.85	78.01
40:60 (42 weeks)	0.86	77.72
40:60 (43 weeks)	0.86	77.81
40:60 (51 weeks)	0.87	79.95
40:60 (67 weeks)	0.89	83.09
40:60 (80 weeks)	0.87	87.58
40:60 (84 weeks)	0.86	88.86
80:20 (41 weeks)	0.85	102.31
80:20 (42 weeks)	0.86	100.86
80:20 (43 weeks)	0.86	99.73
80:20 (51 weeks)	0.87	92.2
80:20 (67 weeks)	0.89	73.29
80:20 (80 weeks)	0.87	73.2
80:20 (84 weeks)	0.86	75.9
ARM (τ in weeks)	**Pearson's correlation coefficient**	**cumulative residual**
L2 (42 weeks)	0.85	130.07
L2 (67 weeks)	0.89	91.21
L2 (84 weeks)	0.85	85.26
WF (18 weeks)	0.89	126.28
WS (18 weeks)	0.93	123.18

Table S3 | Correlation and cumulative residual values for BMM and ARM model scenarios at variable karst residence times (τ). Variable τ's were selected for each model based on significantly correlated R values ≥ 0.85 ($p<0.05$).